

Numerical study of infiltration into a soil–geotextile column

T. Iryo¹ and R. K. Rowe²

¹Post-Doctoral Fellow, GeoEngineering Centre at Queen's-RMC, Queen's University, Kingston, Ontario, Canada, K7L 3N6, Telephone: +1 613 533 6000 ext. 77558, Telefax: +1 613 533 2128; E-mail: iryo@civil.queensu.ca

²Professor, Vice Principal (Research), Queen's University, Kingston, Ontario, Canada, K7K 3N6, Telephone: +1 613 533 6933, Telefax: +1 613 533 6934, E-mail: kerry@civil.queensu.ca

Received 15 July 2003, revised 17 March 2004, accepted 19 March 2004

ABSTRACT: The hydraulic response to infiltration of geotextiles embedded in a sandy soil is examined. An experiment examining infiltration in a one-dimensional, homogeneous sand column is simulated using the finite element method, and functions for the hydraulic properties of the unsaturated porous media that incorporate hysteresis are examined. The numerical procedure is used to model infiltration into a sand column containing a geotextile layer, and the numerical results are compared with the experimental data. To provide insight into the hydraulic behaviour of these systems, the calibrated model is then used to perform a series of numerical experiments for different soil and boundary conditions. Finally, based on these results, the hydraulic behaviour of a one-dimensional, soil–geotextile layered system during infiltration is discussed.

KEYWORDS: Geosynthetics, Geotextiles, Infiltration, Unsaturated flow, Hysteresis, Finite element method

REFERENCE: Iryo, T. & Rowe, R. K. (2004). Numerical study of infiltration into a soil–geotextile column. *Geosynthetics International*, 11, No. 5, 377–389

1. INTRODUCTION

In addition to providing reinforcement, nonwoven geotextiles are considered to contribute to the stability of soil structures by dissipating excess porewater pressure caused by construction or infiltration. Reviewing studies of the hydraulic behaviour of geosynthetics and the interaction between geosynthetics and cohesive soil, Zornberg and Mitchell (1994) noted that nonwoven geotextiles perform well as lateral drains within poorly draining fill material. It has also been reported, however, that clean and dry geotextiles work as a moisture barrier (Henry 1998). The fundamental difference between these two functions (i.e. drainage layer or moisture barrier) raises the question as to how these very different roles are linked to the hydraulic behaviour of the geotextiles. When geotextiles provide drainage, the soil surrounding them is usually saturated, and pore pressures are positive. On the other hand, when geotextiles function as a capillary barrier, the soil around them is unsaturated, and porewater is under suction. Thus it is of particular interest to consider the hydraulic behaviour of geotextiles within soil that is subject to infiltration.

Ho (2000) conducted infiltration tests using a one-dimensional sand column containing a geotextile layer to investigate the hydraulic behaviour of a layered soil–

geotextile system during infiltration. Two separate geotextile specimens were used to evaluate the effects of intrusion of soil particles into the geotextile. Specimen no. 1 was a nonwoven needle-punched geotextile as provided by the manufacturer. Specimen no. 2 was a similar geotextile rubbed with kaolin paste to lower the porosity and saturated hydraulic conductivity relative to the untreated specimen (no. 1). This study showed that the development of porewater pressure within the sand column containing the geotextile layer during advance of the wetting front was different from that of a similar sand column without the geotextile layer. Positive porewater pressure developed above the geotextile when the wetting front reached the geotextile layer. The porewater pressure developed above the geotextile increased with decreasing saturated hydraulic conductivity of the geotextile, $k_{\text{sat geotextile}}$. Ho (2000) also conducted a numerical study of his soil–geotextile layered system by solving Richards's equation (Richards 1931) using the finite difference method.

To simulate water flow within unsaturated porous media using Richards's equation, it is necessary to obtain functions for both the water characteristic curve (water content against suction) and the hydraulic conductivity (hydraulic conductivity against suction). Iryo and Rowe (2003) compiled published data relating

to these functions for geotextiles (Stormont *et al.* 1997; Ho 2000; Lafleur *et al.* 2000; Morris 2000; Stormont and Morris 2000; Knight and Kotha 2001). It was concluded that these functions for geotextiles are steeper than those for most types of soil, and that geotextiles may perform like coarse materials such as gravel. Iryo and Rowe (2003) also evaluated a finite element implementation of Richards's equation for modelling unsaturated flow within a soil-geotextile layered system.

The objective of this paper is to examine the suitability of a finite element formulation for modelling this problem and then to use the model to examine the hydraulic behaviour of geotextiles within the soil under infiltration by performing numerical experiments. The study reported herein has four components. First, infiltration in a one-dimensional homogeneous sand column is modelled using experimentally determined functions for the hydraulic properties of the unsaturated porous media that incorporate hysteresis to examine the suitability of these functions for further study. Second, the model is employed to simulate infiltration into a one-dimensional sand column now containing a single geotextile layer. The results are then compared with experimental results obtained by Ho (2000). Third, numerical experiments are conducted for different soil and boundary conditions to provide insight into the hydraulic behaviour of such a system. Finally, the hydraulic behaviour of the one-dimensional layered soil-geotextile system subjected to infiltration is discussed based on the findings from this numerical study.

2. NUMERICAL SIMULATION OF A ONE-DIMENSIONAL INFILTRATION TEST FOR A SAND COLUMN CONSIDERING HYSTERESIS

The governing equation for transient water flow within an unsaturated soil, as derived by Richards (1931), has been widely used. This equation, obtained from Darcy's law of flow and continuity, can be expressed as

$$k_x \frac{\partial^2 h}{\partial x^2} + k_y \frac{\partial^2 h}{\partial y^2} = \frac{\partial \theta}{\partial t} = m_w \gamma_w \frac{\partial h}{\partial t} \quad (1)$$

for a two-dimensional homogeneous anisotropic material, where: h = total hydraulic head; k_x , k_y = hydraulic conductivity in the x -direction and y -direction respectively; m_w = coefficient of water volume change (slope of the water characteristic curve); γ_w = unit weight of water; θ = volumetric water content; t = time.

Many studies of flow through unsaturated soil have revealed that k and m_w are material specific, and both are dependent on pore pressure. Therefore having appropriate functions is essential for the study of water flow within unsaturated soil. Although hysteresis of hydraulic behaviour of soil is often ignored, the evidence suggests that functions considering either the wetting phase or full hysteresis should be used instead of drying phase functions to study soil water flow (Whistler and Watson 1969; Dane and Wierenga 1975; Stauffer and Darcos

1984; Kaluarachchi and Parker 1987). A relatively simple approach for considering the hysteretic hydraulic behaviour of soil has been proposed by Kool and Parker (1987). This approach is used in the present paper to study infiltration into a one-dimensional soil column with and without a single geotextile layer, and the numerical results are compared with the experimental findings of Ho (2000).

2.1. Functions for hydraulic properties considering hysteresis

2.1.1. van Genuchten-Mualem's equations

van Genuchten (1980) suggested a simple three-parameter equation to describe the water characteristic curve:

$$\Theta = \frac{\theta - \theta_r}{\theta_s - \theta_r} = \left\{ \frac{1}{1 + [\alpha(s/\gamma_w)^n]} \right\}^m \quad (2)$$

where θ_s , θ_r = the saturated water content and the residual water content respectively; Θ = normalised water content; s = suction; and α , n , m are fitting parameters.

Based on the water characteristic curve (Equation 2) assuming $m = 1 - 1/n$, and Mualem's (1976) model of hydraulic conductivity function, which requires a water characteristic curve and saturated hydraulic conductivity, a commonly used hydraulic conductivity function is given by

$$k_r(\Theta) = \frac{k(\Theta)}{k_{sat}} = \Theta^{1/2} \left[1 - (1 - \Theta^{1/m})^m \right]^2 \quad (3)$$

where k_r = the relative hydraulic conductivity; $k(\Theta)$ = the hydraulic conductivity at given Θ ; and k_{sat} = the saturated hydraulic conductivity.

2.1.2. Kool and Parker (1987) hysteretic model

Kool and Parker (1987) assumed that the scanning drying and wetting water characteristic curves could be obtained using the same model and parameters as used for the main curves (i.e. the scanning curves are scaled-down versions of the primary curves). Figure 1 shows a schematic representation of the main drying and wetting curves and a scanning wetting curve considering entrapped air. To force the scanning curves through the reversal point (i.e. the point where the scanning curve starts) either θ_s or θ_r is modified as described in the following paragraphs.

For the drying scanning curve, θ_r from the main curves is used, but θ_s is replaced by the modified value θ_s^* given by

$$\theta_s^* = \frac{\theta_\Delta - \theta_r [1 - \Theta^d(s_\Delta)]}{\Theta^d(s_\Delta)} \quad (4)$$

where θ_Δ = water content at the reversal point; $\Theta^d(s_\Delta)$ = normalised water content on the main drying curve at the reversal point; and s_Δ = suction at the reversal point. Thus the drying scanning curves are obtained from Equation 2 using θ_r and θ_s^* in addition to the fitting parameters for the main drying curve, n^d , α^d .

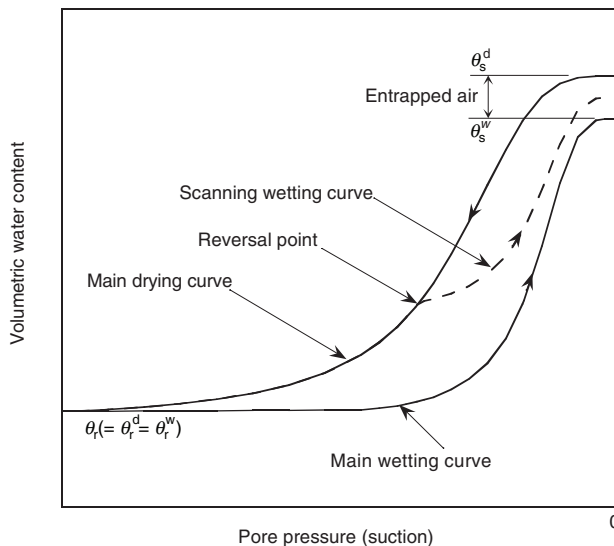


Figure 1. Schematic water characteristic curve considering hysteresis and entrapped air

For the wetting scanning curve, the original saturated water content from the main curves remains, and residual water content is replaced by modified value θ_r^* . For the wetting scanning curve, θ_s from the main curves is used, but θ_r is replaced by the modified value θ_r^* given by

$$\theta_r^* = \frac{\theta_\Delta - \theta_s \Theta^w(s_\Delta)}{1 - \Theta^w(s_\Delta)} \quad (5)$$

where $\Theta^w(s_\Delta)$ = normalised water content on the main wetting curve at the reversal point. The drying scanning curves are obtained by Equation 2 using θ_r^* and θ_s in addition to the fitting parameters for the main wetting curve, n^w, α^w .

It is very common to encounter air entrapped in the soil during infiltration, and this entrapped air may occupy between 0% and 20% of the porosity (Fayer and Hillel 1986). Thus, in this study, some air was assumed to be entrapped in the soil column during the infiltration experiments. Thus the value of θ_s used in this study was smaller than the soil porosity, n_p .

The hydraulic conductivity function is estimated using the water characteristic curve obtained by the hysteretic model described above and Equation 3, assuming that hysteresis between hydraulic conductivity and water content is small enough to be ignored.

2.2. Infiltration into a one-dimensional sand column

2.2.1. The experiment

Ho (2000) conducted physical experiments to examine the hydraulic behaviour of a one-dimensional sand column, and a sand column containing a single horizontal layer of geotextile (sand–geotextile column) under infiltration loading. Infiltration into the sand column without the geotextile (referred to as Case 1 in this study) is numerically simulated in this section to examine the functions for the hydraulic properties considering hysteresis. Ho’s column was a hollow Plexiglas cylinder, 0.1 m in diameter by 2.15 m long,

Table 1. Properties of sand (Ho 2000)

Parameter	Value
Particle size at 10% passing by mass, D_{10} (mm)	0.13
Particle size at 30% passing by mass, D_{30} (mm)	0.27
Particle size at 60% passing by mass, D_{60} (mm)	0.6
Porosity, n_p	0.52
Saturated hydraulic conductivity, k_{sat} (m/s)	2.04×10^{-3}

containing soil. A datum was established 0.2 m above the bottom of the column. Pore pressure was measured along the column. Soil extraction ports were located along the column to recover soil specimens for water content measurements. The soil used for this experiment was a well-graded sand with physical properties as summarised in Table 1. The sand layer was formed by dropping the sand particles into a column filled by water. Thus, after placement, the sand was loose and saturated. To create an initial condition for the subsequent infiltration test, the column was drained from the bottom for 20 min. After 20 min, a relatively uniform pore pressure with an average value of $-0.11 \text{ mH}_2\text{O}$ (-1.08 kPa) was distributed along the column from the top to the bottom. All infiltration tests were commenced after the 20 min drainage and sustained by a constant 0.1 m head on the top of the soil column.

2.2.2. The numerical simulation

The numerical simulations were carried out by solving Equation 1 using the finite element method as implemented in the program SEEP/W v. 5 (GEO-SLOPE 2001). As the properties k and m_w are both functions of pore pressure, Equation 1 is solved using an iterative scheme. The column was modelled using 398 four-noded rectangular elements with height of 0.005 m except near the geotextile, as shown in Figure 2. The program is designed for two-dimensional analysis, and the sand column and geotextile were modelled with a single column of two-dimensional elements by applying a zero horizontal flux boundary condition to both sides of the column. This forced the flow to be vertical and hence one-dimensional. For Case 1 there was no geotextile, and the elements intended to model the geotextile were given the properties of sand for these simulations. The initial condition was a uniform distribution of the pore pressure head of -0.11 m along the column. A 0.1 m pressure head was specified at the top of the column. The experimental data (Ho 2000) showed that nearly hydrostatic pressure was developed along the column after the wetting front reached the datum. Thus a no flux boundary condition was also specified at the bottom of the modelled column. The time step was automatically varied from 0.001 to 1 s using the adaptive time-stepping routine incorporated into the program.

The scanning wetting water characteristic curve and the hydraulic conductivity function obtained using Kool and Parker’s model are used as the functions for the hydraulic properties of the sand. To obtain these hydraulic functions, the measured water content and

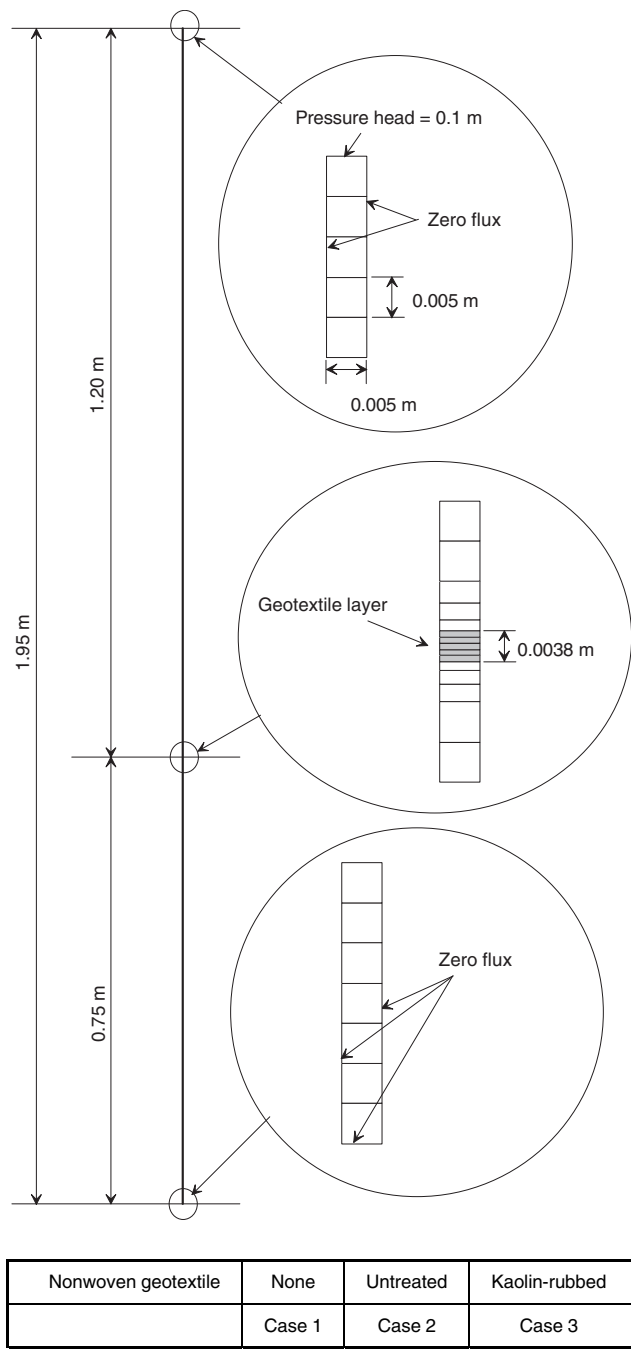


Figure 2. Infiltration experiments modelled

the pore pressure data along the column after 20 min of drainage were first fitted by van Genuchten equations using the program RETC (van Genuchten *et al.* 1991). θ_s^d is equal to the porosity of this sand column ($\theta_s^d = 0.52$). Using RETC, the parameters $\alpha^d (= \alpha^d / \gamma_w) = 1.27 \text{ kPa}^{-1}$, $n^d = 7.00$ and $\theta_r^d = 0.16$ were deduced, and the main drying curve obtained from these parameters is shown as a dashed line in Figure 3a together with the measured data. Although the range of the suction for the measured data was small, the range covered the suction during infiltration. Thus the use of parameters derived from the data after 20 min drainage was considered to be reasonable for simulating infiltration.

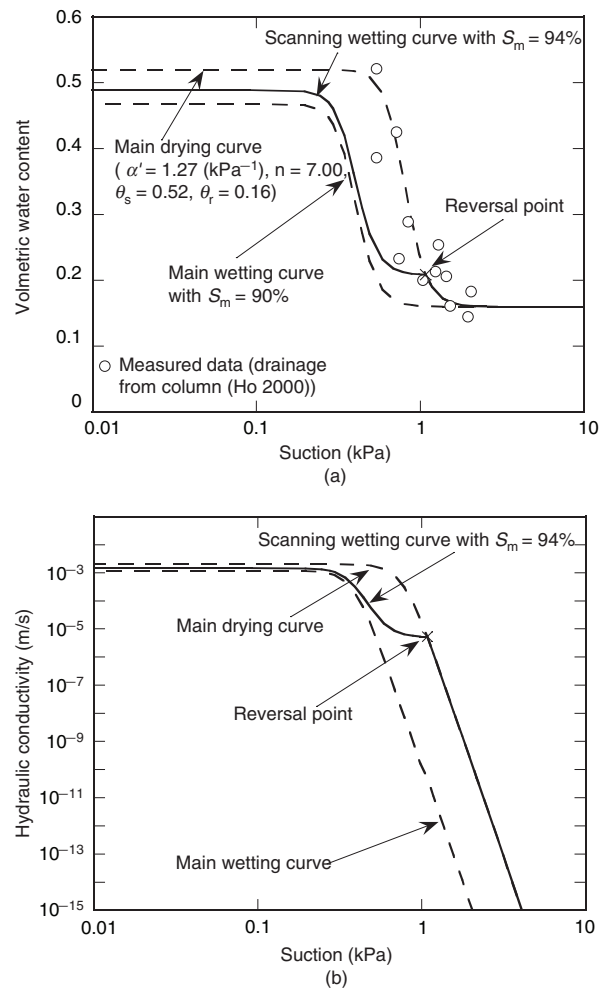


Figure 3. Hydraulic properties for sand: (a) water characteristic curves; (b) hydraulic conductivity functions

Kool and Parker compared the measured main drying and wetting water characteristic curves for eight different soils. They found that one of the fitting parameters for the wetting curve, n^w , may be approximated by that for the drying curve (i.e. $n^w = n^d$), and another parameter, α^w , may be approximated by $\alpha^w = 2 \times \alpha^d$. These relationships have been used for studies by Luckner *et al.* (1989) and Lenhard *et al.* (1991). Using these relationships, the main wetting curve, required by the Kool and Parker model to obtain scanning curves, is defined by $\alpha^w = 2 \times \alpha^d = 2.548 \text{ kPa}^{-1}$, $n^w = n^d = 7.00$ and $\theta_r^w = \theta_r^d = 0.16$. Although entrapped air was expected, the amount of air was not measured, and so the value of θ_s^w was obtained from a parametric study that considered the following values of S_m : 90%, 92%, 94%, 96% and 100%. The pore pressure at the reversal point is equal to the initial pore pressure prior to the infiltration test (i.e. $-0.11 \text{ H}_2\text{O}$ or -1.08 kPa). The scanning wetting curve is obtained from these parameters based on Equations 2 and 5. The scanning wetting curve assuming the maximum degree of saturation, $S_m = 94\%$ (i.e. 6% of voids are occupied by entrapped air) is shown in Figure 3a by a solid line as an example of the curve obtained from the Kool and Parker model. The main wetting

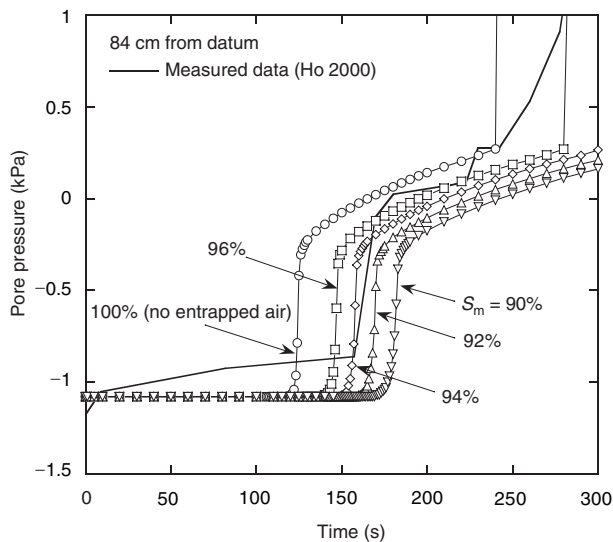


Figure 4. Pore pressure development at 84 cm above datum for Case 1

curve with $S_m = 90\%$ is also shown in this figure as the other dashed line.

Hydraulic conductivity functions estimated from the water characteristic curves in Figure 3a and Equation 3 are shown in Figure 3b.

2.2.3. Comparison of experimental and numerical results

The development of pore pressure at a location 84 cm above the datum is shown in Figure 4. The experimental results are shown as a solid line, and the numerical results are shown as solid lines with symbols. According to the experimental results, the pore pressure increased twice during this infiltration test. The first increase occurred at about 150 s and the second increase occurred at about 250 s. The first increase was due to the wetting front passing the monitoring point, and the second increase was caused by the hydrostatic pressure developed within the column after the wetting front reached the datum. Because the development of the pore pressure due to an impermeable layer below the soil-geotextile system is beyond the scope of this study, subsequent discussion focuses only on the first increase in pore pressure. The experimental results show that the pore pressure was relatively constant at about -1 kPa from the beginning of infiltration. When the wetting front reached the monitoring point, the pore pressure suddenly increased from a negative value to about 0 kPa. The pore pressure profile along the column is shown for four different times in Figure 5. It is evident that the wetting front occupies a narrow zone.

The development of the pore pressure obtained from the numerical simulations is also shown in Figure 4. The numerical results show that the pore pressure was constant at the initial value until it increased to about 0 kPa, when the wetting front passed. The increase occurred very rapidly as observed for the experimental result. The pore pressure increase occurred later as the value of S_m was reduced. This is because the hydraulic conductivity of soil, k_{soil} , is reduced for smaller values of

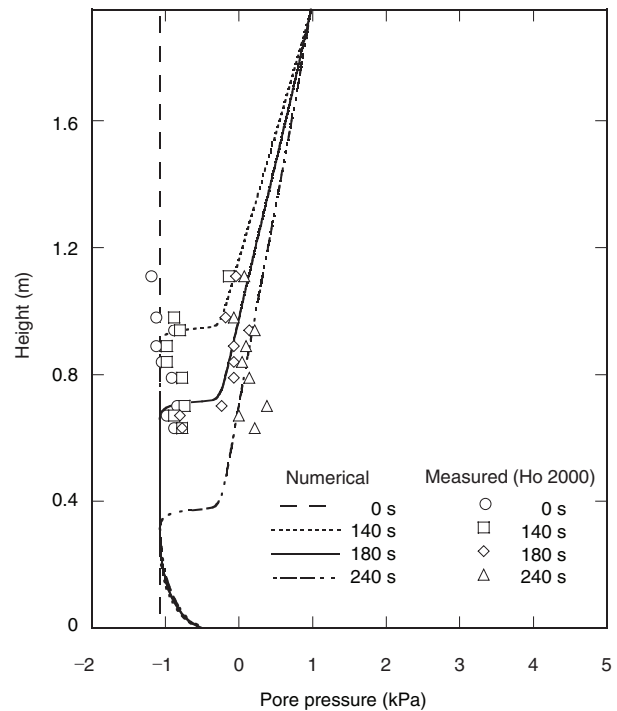


Figure 5. Pore pressure profiles for Case 1

S_m , and, as a result, infiltration will advance more slowly. Of the several values of S_m used for this simulation, $S_m = 94\%$ gave the best agreement with the experimental result with respect to the time of the first pore pressure increase. Pore pressure profiles obtained from the numerical simulation with $S_m = 94\%$ are shown in Figure 5. The advance of the wetting front was evident, and the pore pressures were almost linearly distributed from the top of the column to the wetting front. The accuracy of the numerical simulation was examined by comparing the difference between the numerically and experimentally deduced changes in pore pressure. The mean difference based on all monitoring points was found to be about 9%. Thus it is considered that the numerical simulation reproduced the infiltration into the sand column reasonably well, and the functions for the hydraulic properties with $S_m = 94\%$ were used for the remainder of this study.

3. NUMERICAL SIMULATION OF INFILTRATION INTO ONE-DIMENSIONAL SAND-GEOTEXTILE COLUMN

In this section, infiltration into a one-dimensional sand column containing a geotextile is numerically simulated using the same numerical procedure as that adopted for simulating infiltration into the sand column described in the previous section. The results are then compared with the experimental result obtained by Ho (2000) to assess its applicability for modelling a soil-geotextile system.

Table 2. Properties of geotextiles (Ho 2000)

Parameter	Nonwoven (untreated)	Nonwoven (kaolin-rubbed)
Thickness, $t_{\text{geotextile}}$ (mm)	3.80	3.80
Porosity, n_p	0.86	0.32
Saturated hydraulic conductivity, k_{sat} (m/s)	1.45×10^{-3}	4.75×10^{-4}

3.1. Ho's (2000) experiments

The sand columns with geotextiles were prepared using the same procedure as for the sand column described earlier except that a horizontal, circular geotextile specimen was located 0.95 m above the bottom of the column. Two separate needle-punched nonwoven (Amoco 4516) specimens were examined. The first untreated specimen was as provided by the manufacturer. To evaluate the effects of intrusion of soil particles into the geotextile, the second specimen was rubbed with kaolin paste. The experiment with the untreated geotextile is referred to as Case 2, and the experiment with the kaolin-rubbed geotextile is referred to as Case 3. The kaolin-rubbed specimen had a lower n_p and $k_{\text{sat geotextile}}$ than the untreated specimen (see Table 2). The infiltration commenced following 20 min drainage from a fully saturated column. Hence the sand columns and geotextiles were relatively dry prior to the infiltration tests (i.e. their water contents were close to the residual values).

3.2. The numerical simulations

The numerical procedure used to simulate infiltration into the sand–geotextile column was the same as that described in the previous section for the sand column (Case 1). The finite element mesh was identical to that used earlier for Case 1, but five four-noded rectangular elements previously assigned sand properties were used here to model the geotextile and were assigned geotextile properties as discussed below. The initial and boundary conditions were the same as described for Case 1. The functions for the hydraulic properties of the sand are those obtained in previous section with $S_m = 94\%$. The functions for the hydraulic properties of geotextiles, both untreated (Case 2) and kaolin-rubbed (Case 3), were obtained using the same procedure as described for sand. The experimental data for the main drying water characteristic curves of the geotextiles were obtained by Ho (2000) using a suction plate apparatus and an overburden pressure equivalent to the pressure caused by sand above the geotextile specimens within the column. The value of $k_{\text{sat geotextile}}$ for both geotextiles were also reported by Ho (2000). The values of θ_s^w for the geotextiles were obtained based on parametric studies, as the amount of entrapped air was not measured.

Measured data for the main drying water characteristic curves of untreated and kaolin-rubbed geotextiles are shown in Figures 6a and 7a together with the curves fitted by the van Genuchten equations using the program RETC. Although there is no experimental confirmation for geotextiles, the main wetting curves were approximated as described earlier for the sand

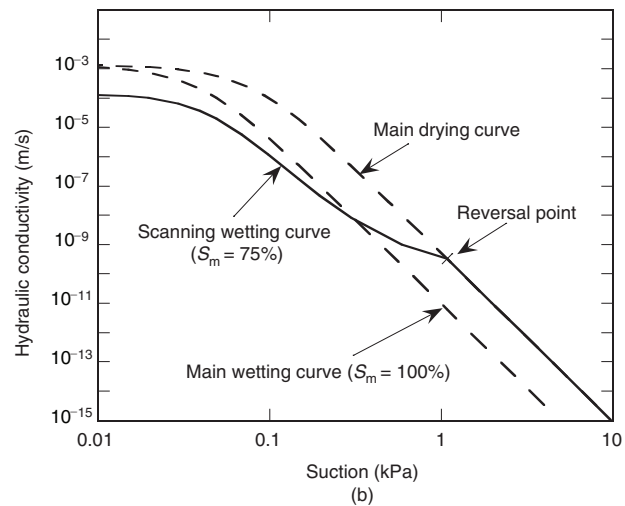
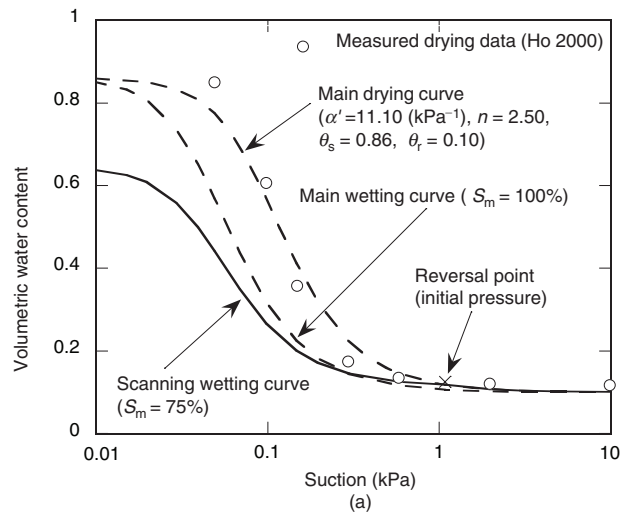


Figure 6. Hydraulic properties for untreated geotextile: (a) water characteristic curves; (b) hydraulic conductivity functions

($\alpha^w = 2 \times \alpha^d, n^w = n^d$) and are also shown in these figures. Further investigation on this issue is recommended. The main wetting curves show that the water entry values (water intrudes into the media and fills the voids below this value of suction) for both untreated and kaolin-rubbed geotextiles are about 0.2 kPa. The hydraulic conductivity functions associated with these water characteristic curves are shown in Figures 6b and 7b.

3.3. Comparison of experimental and numerical results

The measured pore pressure profiles for Case 3 obtained by Ho (2000) are shown in Figure 8. The pore pressure profiles shown in this figure are for 0 s (the beginning of the infiltration), 140 s (just before the wetting front reached the geotextile layer), 180 s (just after the wetting

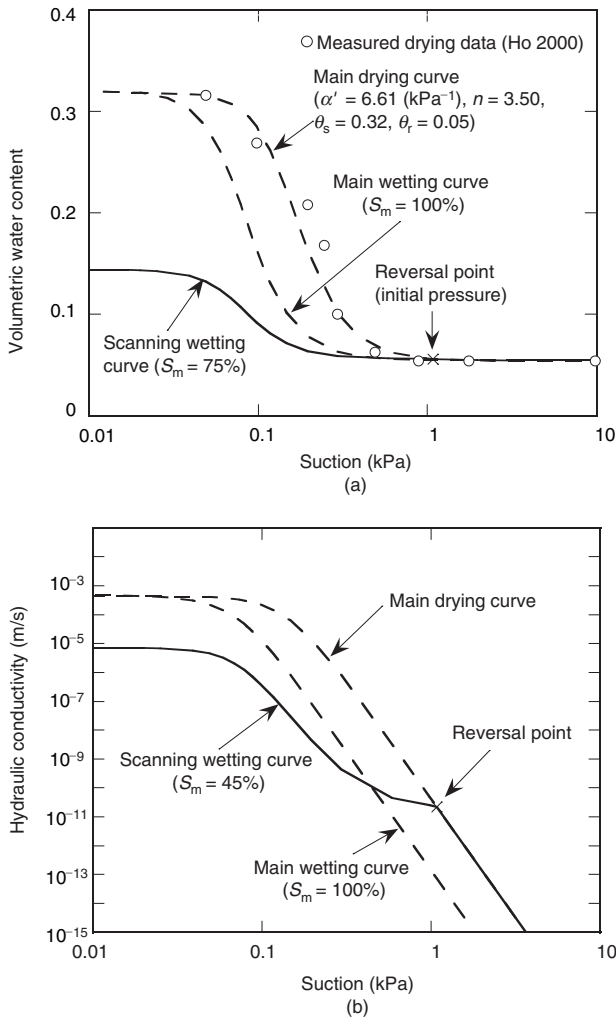


Figure 7. Hydraulic properties for kaolin-rubbed geotextile: (a) water characteristic curves; (b) hydraulic conductivity functions

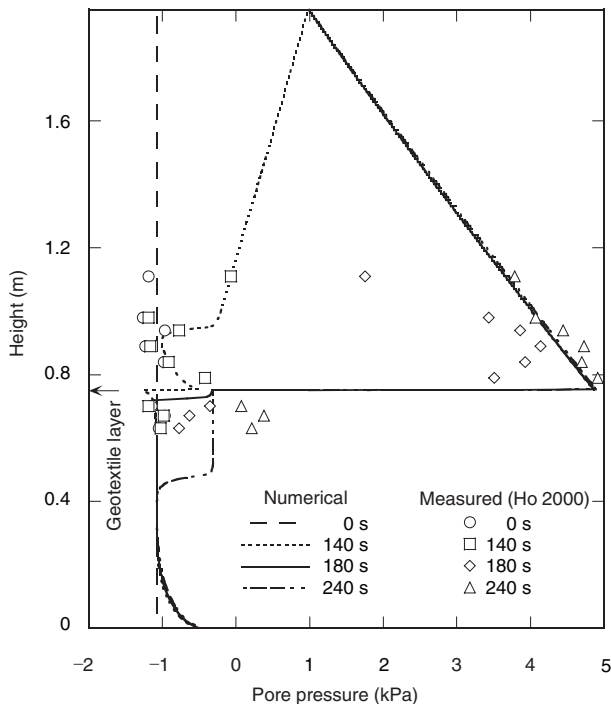


Figure 8. Pore pressure profiles for Case 3

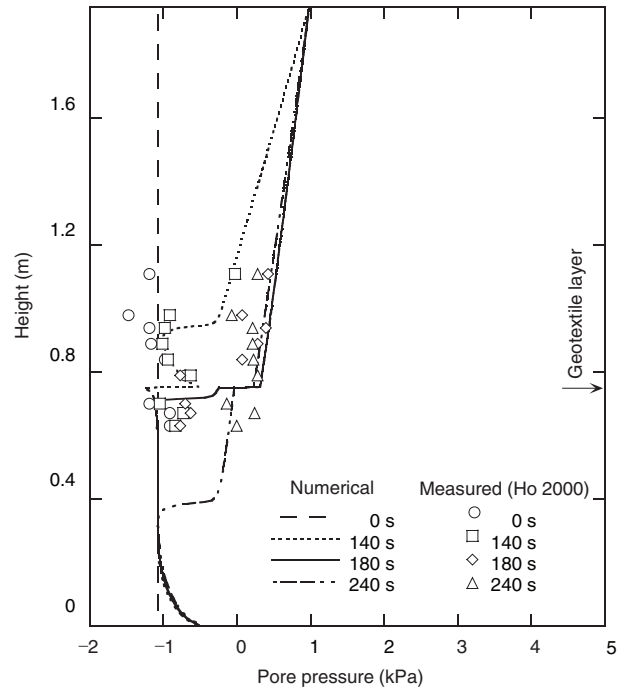


Figure 9. Pore pressure profiles for Case 2

front reached the geotextile layer), and 240 s (well after the wetting front passed the geotextile layer but before it reached the datum).

The experimental data show that the advance of the wetting front was observed both above and below the geotextile layer. It is also observed that, once the wetting front reached the geotextile layer, high pore pressures developed above the geotextile layer, but not below. Thus the pore pressure profiles were discontinuous at the geotextile layer. Experimental results for Case 2 (Figure 9) showed a similar response although the pore pressures above the geotextile were much smaller than for Case 3.

It was expected that some air was entrapped in the geotextile during the infiltration in a similar manner as assumed for sand. Thus numerical simulations were conducted for a variety of values of S_m for the geotextiles for both Cases 2 and 3. It is found that higher pore pressure above the geotextile can be obtained by considering entrapped air. The best ‘predictions’ of pore pressure were obtained for $S_m = 75\%$ in Case 2, and 45% in Case 3. The scanning wetting water characteristic curve obtained by Kool and Parker’s model for Case 2 with $S_m = 75\%$, and that of Case 3 with $S_m = 45\%$ are shown in Figures 6a and 7a, and the hydraulic conductivity functions obtained from these water characteristic curves are shown in Figures 6b and 7b.

The results of the numerical simulations considering these values of S_m are shown in Figures 8 and 9. In Cases 2 and 3, both experimental data and the numerical results at 140 s indicate that the initial condition (uniform distribution of pore pressure) was not in equilibrium, and that some gravity-driven migration of water occurred prior to the arrival of the wetting front.

Increases in pore pressure caused by the advance of the wetting front were reproduced by the numerical simulations. The higher pore pressure above the geotextile layer and the discontinuity of pressure profiles also showed good agreement with the experimental results. These pore pressure profiles indicate that the geotextiles within the sand column behaved as a lower-permeability material than the sand, both before and after the wetting front had passed the geotextile layer.

4. NUMERICAL EXPERIMENT OF INFILTRATION INTO ONE-DIMENSIONAL LOAMY SAND-GEOTEXTILE COLUMN

4.1. The numerical experiments

The physical experiments simulated in the previous section examined the case where the saturated hydraulic conductivity for soil, $k_{sat\ soil}$, is larger than $k_{sat\ geotextile}$, and this relationship held over the entire suction range. However, it is also necessary to see how the soil-geotextile system responds hydraulically when $k_{sat\ soil}$ is smaller than $k_{sat\ geotextile}$, as nonwoven geotextiles are often used for drainage purpose within less permeable soil. The soil to be examined in the following is loamy sand with properties as given in Table 3 (deduced from Schaap and Leij 1998). The geotextile was assumed to be an untreated nonwoven geotextile with $S_m = 75\%$ as examined in Case 2. The numerical experiments were conducted for a variety of ‘rainfall’ intensities applied on the top of the column. Case 4 assumed a pressure head of 0.1 m above the soil, and represented an intensity of rainfall greater than $k_{sat\ soil}$ such that a 0.1 m pond developed as simulated in Ho’s experiment. Cases 5 to 9 represented rainfall intensities less than $k_{sat\ soil}$ (i.e. no ponding) and involved a specified flux boundary condition for fluxes, q , of 0.1, 0.15, 0.2, 0.35 and $0.5 \times k_{sat\ soil}$ respectively as summarised in Table 4. In addition to these cases, infiltration into soil columns (without geotextile) was also analysed for comparison purposes. Initial conditions corresponded to a degree of saturation, $S_r = 34\%$, or a pore pressure of -18.4 kPa , uniformly distributed along the column. The water characteristic curves and the hydraulic conductivity functions for the loamy sand and the geotextile are shown in Figure 10a

Table 3. Properties of loamy sand (based on Schaap and Leij 1998)

Parameter	Value
Porosity, n_p	0.39
Saturated hydraulic conductivity, k_{sat} (m/s)	1.2×10^{-5}

Table 4. Numerical experiments: cases considered

Case no.	5	6	7	8	9	4
q (mm/h)	4.4	6.5	8.7	15.3	21.8	0.1 m pressure head
Ratio to $k_{sat\ soil}$	0.10	0.15	0.20	0.35	0.50	

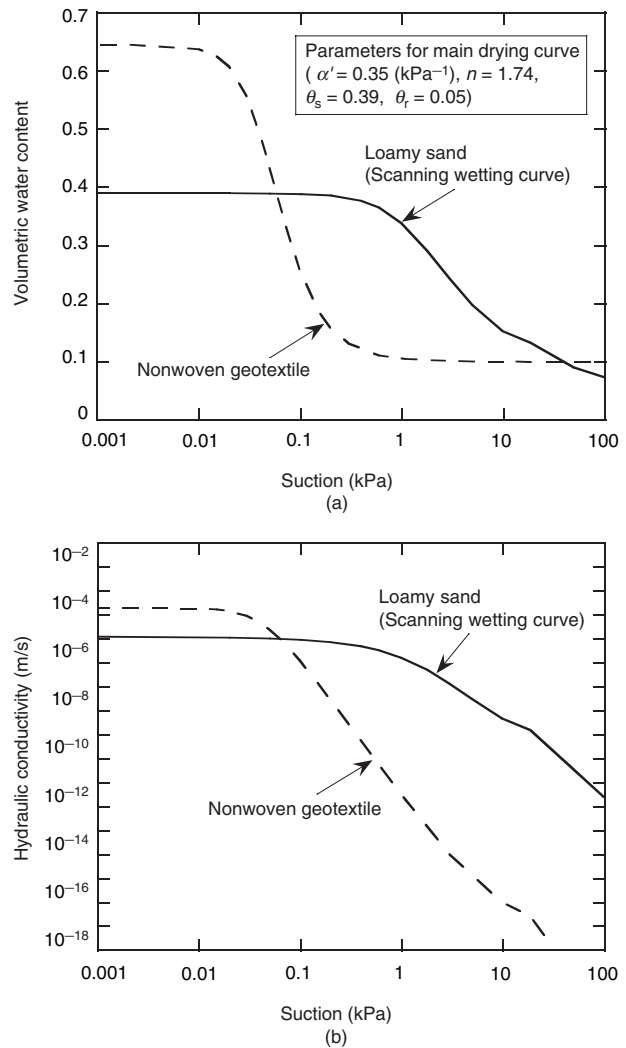


Figure 10. Hydraulic properties for numerical experiment: (a) water characteristic curves; (b) hydraulic conductivity functions

and 10b respectively. Unlike Ho’s experiment, here the hydraulic conductivity curves cross (at around 0.06 kPa).

4.2. Results and discussion

4.2.1. Specified head on the soil column (ponding case)

The pressure profiles of Case 4 are shown in Figure 11. These pressure profiles correspond to before the wetting front reached the geotextile layer (14,000 s), when the wetting front was halted and the maximum pore pressure developed above the geotextile (18,870 s), and after the wetting front had passed the geotextile (26,000 s). The advance of the wetting front is observed both above and below the geotextile layer. Higher pore pressure also developed above the geotextile layer. However, unlike Cases 2 and 3, the high pore pressure above the geotextile layer dissipated after the wetting front had

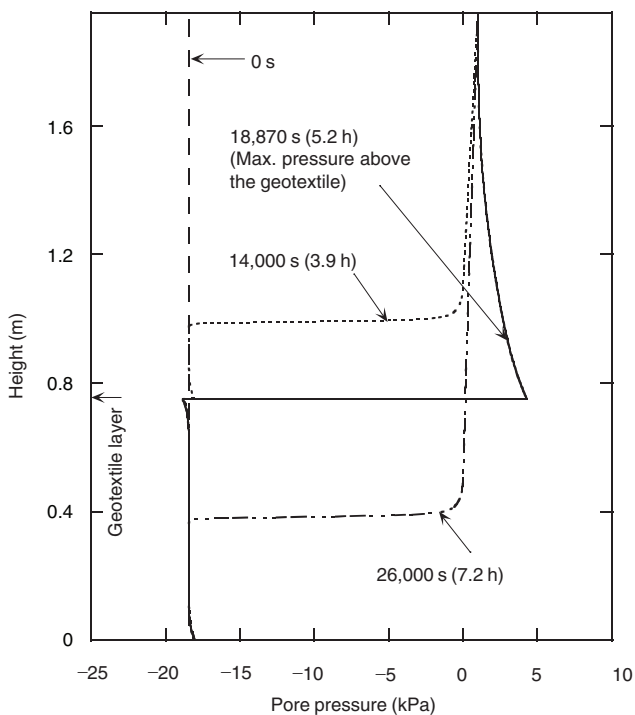


Figure 11. Pore pressure profiles for Case 4

passed the geotextile layer. Thus there was no discontinuity in the pore pressure profile at the geotextile after the wetting front had passed. This indicates that, after passage of the wetting front, the geotextile worked as a more permeable material than the soil in this case. The pressure change above and below the geotextile layer with time is shown in Figure 12. The pore pressures above the geotextile layer increased when the wetting front reached the geotextile layer, and then it decreased with subsequent time as the pore pressures below the geotextile layer increased (i.e. as the wetting front passed through the geotextile layer). The pore pressure change for the case without the geotextile at the same location is referred to as 'below geotextile layer' for the case with a geotextile that is also shown. The pore pressure increase

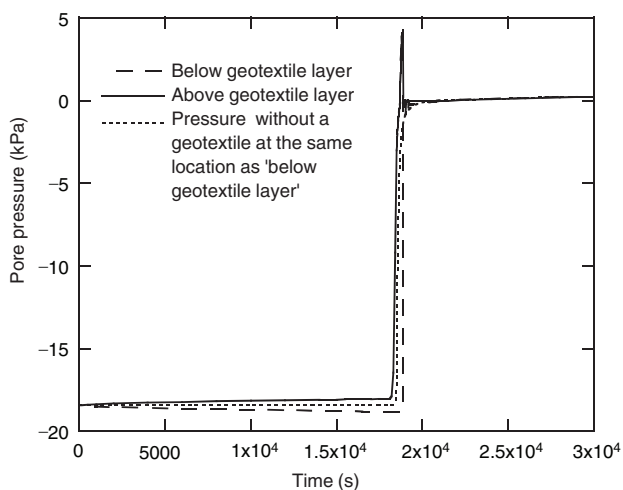


Figure 12. Pore pressure developments around geotextile layer for Case 4

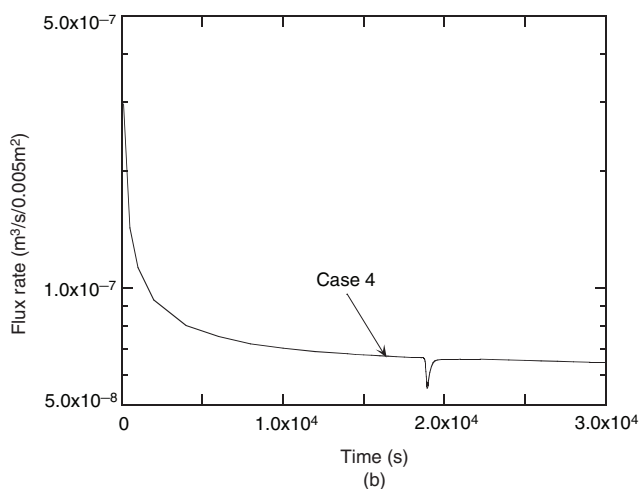
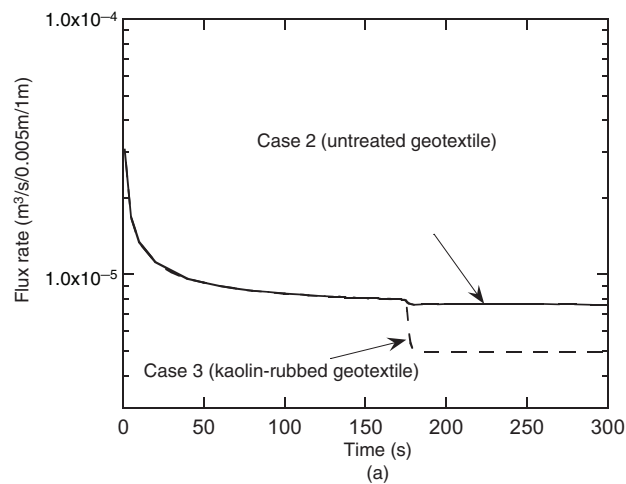


Figure 13. Flux rate at the top of column obtained from numerical simulation: (a) Cases 2 and 3; (b) Case 4

for Case 4 occurred marginally later than that of the case without the geotextile. It is clear that the geotextile layer temporarily halted the advance of the wetting front.

Calculated flux rates at the top of the column for Cases 2 and 3 are shown in Figure 13a and that for Case 4 is shown in Figure 13b. In all cases, the flux rates tended to decrease with time from the beginning, and they decreased suddenly when the wetting front reached the geotextile layer. After they fell, they remained at the reduced rate for Cases 2 and 3, but increased back to essentially the original value for Case 4. This flux rate behaviour for Case 4 is similar to that reported by Miller and Gardner (1962) for a one-dimensional soil column having a thin horizontal layer of coarser soil in a column of otherwise finer soil.

4.2.2. Specified flux on the soil column (no ponding case)

The pore pressure profiles for Case 5 (no ponding) are shown in Figure 14. These pressure profiles correspond to before the wetting front reached the geotextile layer (140,000 s), when the wetting front was halted and the maximum pore pressure developed above the geotextile (220,000 s), and after the wetting front had passed the geotextile (250,000 s). The advance of the wetting front was observed both above and below the geotextile layer.

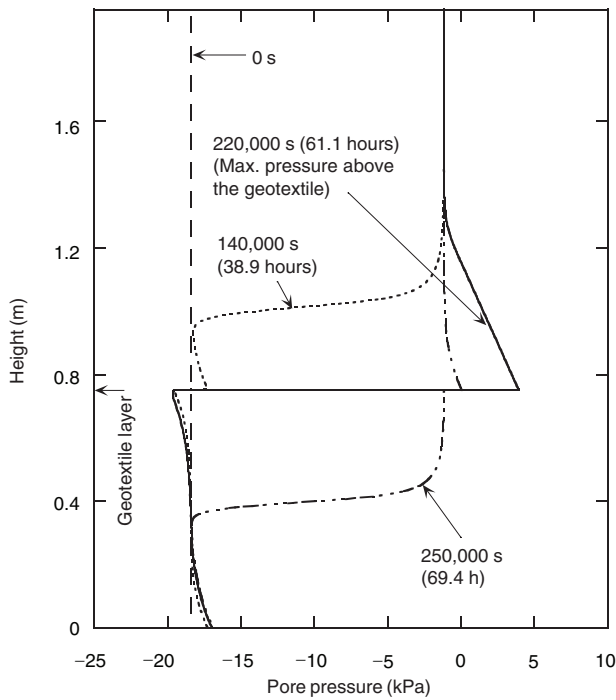


Figure 14. Pore pressure profiles for Case 5

When the wetting front reached the geotextile layer, higher pore pressure developed above the geotextile layer. After the wetting front passed the geotextile layer, the previous positive pore pressures dropped to about 0 kPa, but this pore pressure was still slightly higher than that below the geotextile layer. As a result, a discontinuity in the pore pressure profile was evident at the geotextile layer. Pore pressure increased with the advance of the wetting front but still remained negative except for the pore pressure developed above the geotextile layer after the arrival of the wetting front. This pore pressure profile is very similar to that observed by Corey (1994) for a soil having a thin coarser soil layer when there is a constant flux boundary condition. It was found that, whereas the pore pressure above the geotextile layer increased, below the geotextile layer it decreased slightly even before the wetting front reached the geotextile layer. This indicated that the water contained within the soil migrated downwards by gravity but was stopped at the geotextile layer (i.e. the geotextile layer worked as an impermeable material at this time).

4.2.3. Discussion of the hydraulic behaviour of the soil–geotextile column

The hydraulic behaviour of the one-dimensional soil–geotextile system described above may be explained by the difference between the hydraulic properties of geotextiles and soils. The water characteristic curves of geotextiles have the following features (Iryo and Rowe 2003):

- the air and water entry values (suction) are very small;
- the water characteristic curves are very steep in both the drying and the wetting phase compared with typical soils.

These features imply that the unsaturated geotextile embedded within unsaturated soil will behave as an impermeable layer until the surrounding soil and geotextile are nearly saturated, as the hydraulic conductivity of an unsaturated porous medium decreases as the water content decreases. Once the geotextile is nearly saturated, it becomes a permeable material, and in the case where $k_{\text{sat geotextile}}$ is larger than $k_{\text{sat soil}}$, the geotextile may become more permeable than the soil. This occurs with a small increase of pore pressure.

Considering the hydraulic properties of geotextiles, the hydraulic behaviour of the unsaturated one-dimensional soil–geotextile system discussed in the previous sections can be explained as follows.

1. *Prior to the arrival of the wetting front at the geotextile layer (for all cases):* The geotextile embedded within the unsaturated soil behaved as an impermeable material.
2. *Arrival of the wetting front at the geotextile layer (for all cases):* Initially water does not enter the geotextile, as the water entry value of the geotextile is less than that of the soil. As a result, the wetting front is halted at the upper surface of the geotextile layer, and the pore pressure increases there until it reaches the water entry value. At that time, water starts to enter the geotextile and the geotextile becomes permeable from its upper surface down. In time the entire geotextile becomes permeable, and the wetting front passes through the geotextile layer.
3. *After passage of the wetting front through the geotextile layer:* The hydraulic performance of the unsaturated one-dimensional soil–geotextile system following passage of the wetting front through the geotextile layer varied from case to case, but was controlled by the type of boundary conditions and the difference between the saturated hydraulic conductivity of the geotextile and soil. These variations, as manifest in the pore pressure profile, can be classified into three categories denoted as Type 1, Type 2 and Type 3. Type 1 is for Cases 2 and 3 with ponding and $k_{\text{sat geotextile}}$ less than $k_{\text{sat soil}}$. Type 2 is for Case 4 with ponding and $k_{\text{sat geotextile}}$ larger than $k_{\text{sat soil}}$. Type 3 is for Cases 5–9 with no ponding and $k_{\text{sat geotextile}}$ larger than $k_{\text{sat soil}}$. The hydraulic behaviour of each type is discussed in the following paragraphs.

- *Type 1 ($k_{\text{sat geotextile}} < k_{\text{sat soil}}$; ponding):* Following passage of the wetting front through the geotextile layer, the hydraulic conductivity for geotextile, $k_{\text{geotextile}}$, and that for soil, k_{soil} , in the vicinity of the geotextile approach their saturated values. In this instance the geotextile is less permeable than the soil. As a result, the pore pressure that had developed above the geotextile layer and the discontinuity of the pore pressure profile at the geotextile layer remain.
- *Type 2 ($k_{\text{sat geotextile}} > k_{\text{sat soil}}$; ponding):* Following passage of the wetting front through the geotextile layer, $k_{\text{geotextile}}$ and k_{soil} in the vicinity of the geotextile approach their saturated values. Thus

the geotextile becomes more permeable material than the soil. As a result, the pore pressure developed above the geotextile layer and the discontinuity of the pore pressure profile at the geotextile layer dissipate.

- *Type 3* ($k_{sat \text{ geotextile}} > k_{sat \text{ soil}}$; no ponding; flux $< k_{sat \text{ soil}}$): Following passage of the wetting front through the geotextile layer, both $k_{\text{geotextile}}$ and k_{soil} in the vicinity of the geotextile layer increase. However, the pore pressure in the soil below the geotextile layer doesn't become positive, as the flux is smaller than $k_{sat \text{ soil}}$. Thus $k_{\text{geotextile}}$ decreases with depth from its saturated value at the upper surface to some lower value at its lower surface. As a result most of the pore pressure that had developed above the geotextile layer dissipates, but a relatively small pore pressure discontinuity remains at the geotextile.

To examine the delay to the advancement of the wetting front at the geotextile, the time required for the wetting front to pass the geotextile layer was obtained and is shown in Figure 15 as a function of boundary flux, q . The time shown by $t_3 - t_1$ in this figure is the difference between when the wetting front arrives at the upper surface of the geotextile, t_1 , and the time that the wetting front passes the geotextile (and the pore pressure above the geotextile decreases), t_3 . The time required for the pore pressure at the upper surface of the geotextile to increase to the water entry value ($t_2 - t_1$) is also shown in this figure. It is evident from Figure 15 that the smaller the flux the longer it takes for the pore pressure to reach the water entry value and the wetting front to cross the geotextile layer.

The results of the numerical experiments discussed here imply that the geotextile layer halted the advance of the wetting front while a high water content zone developed above the geotextile layer. This behaviour occurs even in the case where $k_{sat \text{ geotextile}}$ is larger than

$k_{sat \text{ soil}}$ and hence the geotextile is expected to work as a drainage material against infiltration. Thus considerable care is required when selecting nonwoven geotextiles for use within soil structures if one is to avoid the undesirable development of increased water content.

5. CONCLUSIONS

Infiltration in a one-dimensional soil column involving a geotextile layer was examined. Numerical simulations of the laboratory tests reported by Ho (2000) were performed together with numerical experiments for a variety of soil types and boundary conditions. This study leads to the following conclusions.

- Infiltration in a sand column was simulated well by a finite element formulation that included the effect of both hysteresis and entrapped air on the water characteristics curve.
- The numerical simulation considering the entrapped air within the geotextile reproduced the high pore pressures developed above the geotextile layer. Furthermore, the entire process of the infiltration into the sand-geotextile column was simulated well.
- Numerical experiments showed that positive pore pressures were developed above the geotextile layer even for the case where $k_{sat \text{ geotextile}}$ is larger than $k_{sat \text{ soil}}$. This was caused by the wetting front being temporarily halted at the geotextile layer.
- The advance of the wetting front was halted longer (i.e. the positive pore pressures were maintained longer) for specified flux boundary conditions.

This study shows that geotextiles may obstruct seepage flow under some circumstances. Thus care is required to avoid undesirable development of pore pressure above geotextiles in soil structures during periods of infiltration due to rainfall or other water sources.

ACKNOWLEDGEMENTS

The authors are grateful to Professor R. J. Bathurst of the Royal Military College of Canada for his helpful comments. This research was funded by the Natural Sciences and Engineering Research Council of Canada (NSERC).

NOTATIONS

Basic SI units are given in parentheses.

h	total hydraulic head (m)
k	hydraulic conductivity (m/s)
$k_{\text{geotextile}}$	hydraulic conductivity for geotextile (m/s)
k_r	relative hydraulic conductivity (dimensionless)
k_{sat}	saturated hydraulic conductivity (m/s)
$k_{sat \text{ geotextile}}$	saturated hydraulic conductivity for geotextile (m/s)
$k_{sat \text{ soil}}$	saturated hydraulic conductivity for soil (m/s)

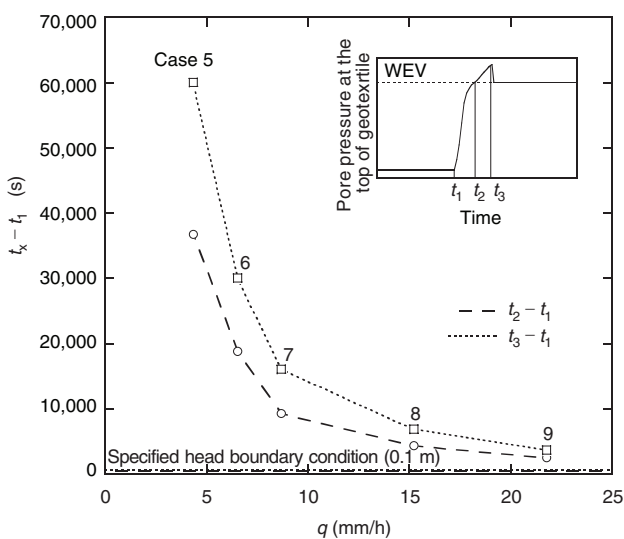


Figure 15. Delay in advance of wetting front by geotextile layer (WEV = water entry value)

k_{soil}	hydraulic conductivity for soil (m/s)	θ_r^*	modified saturated water content for scanning wetting curve (dimensionless)
k_x	hydraulic conductivity in y -direction (m/s)	θ_s	saturated water content (dimensionless)
k_y	hydraulic conductivity in x -direction (m/s)	θ_s^d	saturated water content for main drying curve (dimensionless)
m	fitting parameter for van Genuchten equations (dimensionless)	θ_s^w	saturated water content for main wetting curve (dimensionless)
m_w	coefficient of water volume change (Pa^{-1})	θ_s^*	modified saturated water content for scanning drying curve (dimensionless)
n	fitting parameter for van Genuchten equations (dimensionless)	θ_Δ	water content at reversal point (dimensionless)
n^d	fitting parameter for van Genuchten equations for main drying curve (dimensionless)		
n^w	fitting parameter for van Genuchten equations for main wetting curve (dimensionless)		
n_p	soil porosity (dimensionless)		
q	boundary flux (m^3/s)		
S_m	maximum degree of saturation (dimensionless)		
S_r	degree of saturation (dimensionless)		
s	suction (Pa)		
s_Δ	suction at reversal point (Pa)		
t	time (s)		
t_1	time at which wetting front arrives at upper surface of geotextile (s)		
t_2	time at which pore pressure at upper surface of geotextile increases to water entry value (s)		
t_3	time at which wetting front passes geotextile (s)		
$t_{\text{geotextile}}$	thickness of geotextile (m)		
α	fitting parameter for van Genuchten equations (m^{-1})		
α'	modified fitting parameter for van Genuchten equations (Pa^{-1})		
α^d	fitting parameter for van Genuchten equations on main drying curve (m^{-1})		
α'^d	modified fitting parameter for van Genuchten equations on main drying curve (Pa^{-1})		
α^w	fitting parameter for van Genuchten equations on main wetting curve (m^{-1})		
α'^w	modified fitting parameter for van Genuchten equations on main wetting curve (Pa^{-1})		
γ_w	unit weight of water (N/m^3)		
Θ	normalised water content (dimensionless)		
$\Theta^d(s_\Delta)$	normalised water content on main drying curve at reversal point (dimensionless)		
$\Theta^w(s_\Delta)$	normalised water content on main wetting curve at reversal point (dimensionless)		
θ	volumetric water content (dimensionless)		
θ_r	residual water content (dimensionless)		
θ_r^d	residual water content for main drying curve (dimensionless)		
θ_r^w	residual water content for main wetting curve (dimensionless)		

REFERENCES

- Corey, A. T. (1994). *Mechanics of Immiscible Fluids in Porous Media*, 3rd edn, Water Resources Publications, CO, USA, 252 pp.
- Dane, J. H. & Wierenga, P. J. (1975). Effect of hysteresis on the prediction on infiltration, redistribution and drainage of water in a layered soil. *Journal of Hydrology*, **25**, 229–242.
- Fayer, M. J. & Hillel, D. (1986). Air encapsulation: I. Measurement in a field soil. *Soil Science Society of America Journal*, **50**, 568–572.
- GEO-SLOPE (2001). *SEEP/W Ver.5 User's Guide*, GEO-SLOPE International Ltd, Calgary, Alberta, 539 pp.
- Henry, K. S. (1998). *The Use of Geosynthetics to Mitigate Frost Heave in Soils*, PhD thesis, University of Washington, Seattle, 329 pp.
- Ho, A. F. (2000). *Experimental and Numerical Investigation of Infiltration Ponding in One-dimensional Sand-geotextile Columns*, MSc thesis, Queen's University, Kingston, Ontario, 212 pp.
- Iryo, T. & Rowe, R. K. (2003). On the hydraulic behaviour of unsaturated nonwoven geotextiles. *Geotextiles and Geomembranes*, **21**, No. 6, 381–404.
- Jaynes, D. B. (1984). Comparison of soil-water hysteresis model. *Journal of Hydrology*, **75**, 287–299.
- Kaluarachchi, J. J. & Parker, J. C. (1987). Effects of hysteresis with air entrapment on water flow in the unsaturated zone. *Water Resources Research*, **23**, No. 10, 1967–1976.
- Knight, M. A. & Kotha, S. M. (2001). Measurement of geotextile-water characteristic curves using a controlled outflow capillary pressure cell. *Geosynthetics International*, **8**, No. 3, 271–282.
- Kool, J. B. & Parker, J. C. (1987). Development and evaluation of closed form expressions for hysteresis soil hydraulic properties. *Water Resources Research*, **23**, No. 1, 105–114.
- Lafleur, J., Lebeau, M., Faure, Y., Savard, Y. & Kehila, Y. (2000). Influence of matric suction on the drainage performance of polyester geotextiles. *Proceedings of the 53rd Annual Conference of Canadian Geotechnical Society*, Montreal, Canada, 15–18 October, 2000, Vol. 2, pp. 1115–1122.
- Lenhard, R. J., Parker, J. C. & Kaluarachchi, J. J. (1991). Comparing simulated and experimental hysteretic two-phase transient fluid flow phenomena. *Water Resources Research*, **27**, No. 8, 2113–2124.
- Luckner, L., van Genuchten, M. Th. & Nielsen, D. H. (1989). A consistent set of parametric models for the two-phase flow on immiscible fluids in the subsurface. *Water Resources Research*, **25**, No. 10, 2187–2193.
- Miller, D. E. & Gardner, W. H. (1962). Water infiltration into stratified soil. *Soil Science Society America Proceedings*, **26**, 115–119.
- Morris, C. E. (2000). Unsaturated flow in non-woven geotextiles. *GeoEng2000: An International Conference on Geotechnical and Geological Engineering*, Melbourne, Australia, 19–24 November, 2000, Technomic, Lancaster, PA, USA, Vol. 2, p. 322.
- Mualem, Y. (1976). A new model for predicting the hydraulic conductivity of unsaturated porous media. *Water Resources Research*, **12**, No. 3, 513–522.
- Richards, L. A. (1931). Capillary conduction of liquids through porous mediums. *Physics*, **1**, 318–333.
- Schaap, M. G. & Leij, F. J. (1998). Database-related accuracy and uncertainty of pedotransfer functions. *Soil Science*, **163**, No. 10, 765–779.
- Stauffer, F. & Darcos, T. (1984). Local infiltration into layered soil and response of the water table, experiment and simulation. In *Frontiers in Hydrology* (ed. V. T. Chow), Water Resources Publications, CO, USA, pp. 228–242.
- Stormont, J. C. & Morris, C. E. (2000). Characterization of unsaturated nonwoven geotextiles. In *Advances in Unsaturated Geotechnics* (eds C. D. Shackelford, S. L. Houston and N. Y.

- Chang), ASCE, Proceedings of sessions of Geo-Denver 2000 held in Denver, CO, USA, August 2000, pp. 153–164.
- Stormont, J. C., Henry, K. S. & Evans, T. M. (1997). Water retention functions of four nonwoven polypropylene geotextiles. *Geosynthetics International*, **4**, No. 6, 661–672.
- van Genuchten, M. Th. (1980). A closed-form equation for predicting the hydraulic conductivity of unsaturated soils. *Soil Science Society of America Journal*, **44**, 892–898.
- van Genuchten, M. Th., Leij, F. J. & Yates, S. R. (1991). *The RETC Code for Quantifying the Hydraulic Functions of Unsaturated Soils*, US Environmental Protection Agency Report EPA/600/2–91/065, December 1991.
- Whistler, F. D. & Watson, K. K. (1969). Analysis of infiltration into draining porous media. *Journal of the Irrigation and Drainage*, **95**, No. IR4, 481–491.
- Zornberg, J. G. & Mitchell, J. K. (1994). Reinforced soil structures with poorly draining backfills. Part I: Reinforcement interactions and functions. *Geosynthetics International*, **1**, No. 2, 103–147.

The Editors welcome discussion in all papers published in Geosynthetics International. Please email your contribution to discussion@geosynthetics-international.com by 15 April 2004.